Journal of Orthopaedic Surgery and Research

RESEARCH ARTICLE Open Access

Preliminary study of the role of histone deacetylase (HDAC) in steroid-induced avascular necrosis of the femoral head induced by BMSC adipogenic differentiation

Yong-Le Yu[1], Ping Duan[1], Lin Zheng[1], Jun-Miao Xu[1] and Zhen-Yu Pan[1*]

Abstract

Our previous research revealed a close association between the acetylation of peroxisome proliferator-activated receptor γ (PPARγ) histone H3K27 and the adipogenic differentiation of bone marrow mesenchymal stem cells (BMSCs). We preliminarily explored the epigenetic mechanism of steroid-induced avascular necrosis of the femoral head (SANFH) development, but the specific histone deacetylase (HDAC) involved in this regulatory process remains unknown. In this study, we combined cell, animal, and clinical specimen experiments to screen for specific HDAC genes that could regulate BMSC adipogenic differentiation and to explore their roles. The results showed that dexamethasone (DEX) significantly exacerbated the imbalance between the adipogenic and osteogenic differentiation of BMSCs, and there were differences in HDAC expression in the adipogenic differentiation cell models, with histone deacetylase 10 (HDAC10) showing the most significant decrease in expression. Subsequent use of a chromatin immunoprecipitation assay kit and quantitative polymerase chain reaction (ChIP–qPCR) revealed a decrease in HDAC10 expression at predicted potential sites within the PPARγ promoter, indicating a significant decrease in HDAC10 enrichment in the PPARγ promoter region of BMSCs, thereby promoting sustained PPARγ expression. Additionally, immunohistochemistry of samples collected from mice and humans with SANFH and normal femoral heads revealed an imbalance between adipogenic and osteogenic differentiation in the necrotic area of femoral heads, with a significant decrease in the relative expression of HDAC10 in the necrotic area of femoral heads with SANFH. In summary, we speculate that HDAC10 affects the progression of SANFH by regulating BMSC adipogenic differentiation, a process possibly related to PPARγ histone acetylation. These findings provide a promising direction for the treatment of SANFH.

[†]Yong-Le Yu, Ping Duan and Lin Zheng contributed equally to this work.

*Correspondence:
Zhen-Yu Pan
zn000382@whu.edu.cn

Full list of author information is available at the end of the article

Graphical abstract

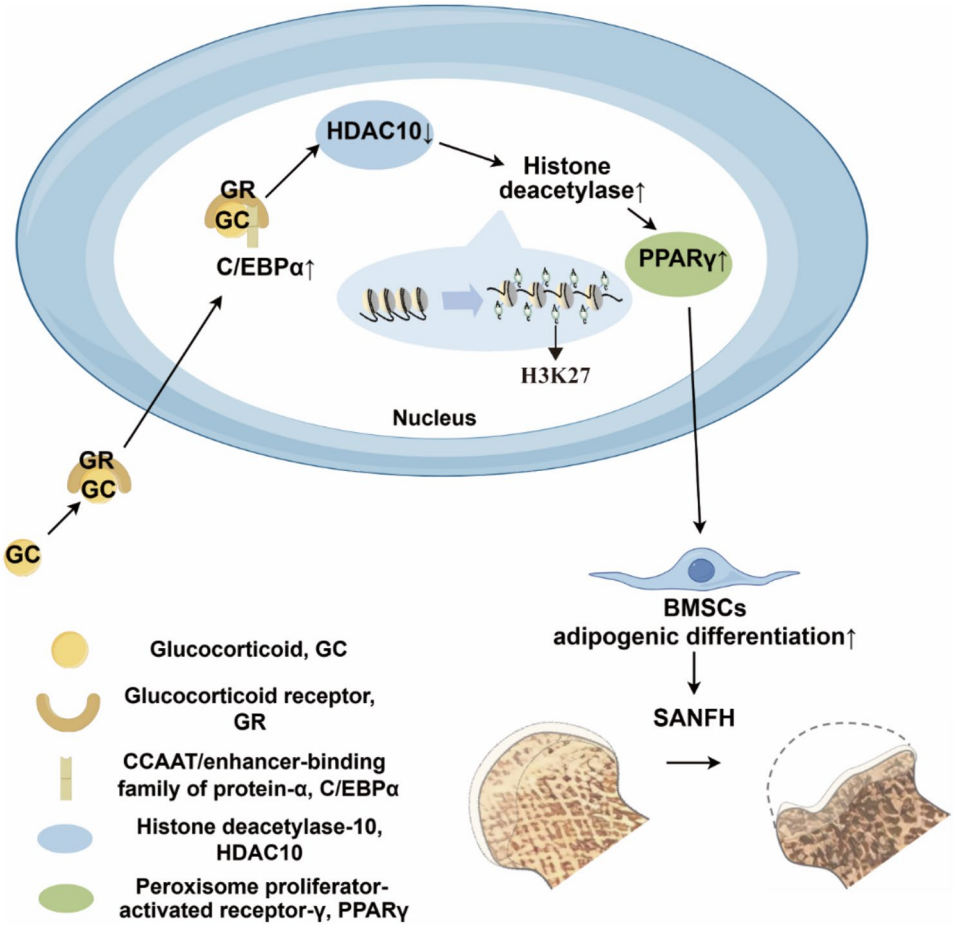

Keywords SANFH, BMSCs, Adipogenic differentiation, Histone deacetylase

Introduction

Steroid-induced avascular necrosis of the femoral head (SANFH) is a common orthopaedic disease [1], with a highly complex pathogenesis involving hypotheses such as disordered fat metabolism, intravascular coagulation, and cell apoptosis [2, 3]. Current treatment options are limited, with advanced stages of the disease typically managed through surgery [4], such as intramedullary decompression [5] or osteotomy [6]. Cell therapy is also used [7], but the overall prognosis remains poor [8]. Research has shown that excessive use of glucocorticoids enhances the adipogenic differentiation of bone marrow mesenchymal stem cells (BMSCs), exacerbating the accumulation of intraosseous fat tissue, blocking blood circulation in vessels, and hindering bone cell repair and reconstruction, ultimately leading to ischaemic necrosis of the femoral head [9]. During the adipogenic differentiation of BMSCs, peroxisome proliferator-activated receptor-gamma (PPARγ) and the CCAAT/enhancer-binding family of proteins (C/EBPs) are key transcriptional regulatory factors [10]. Increased expression of PPARγ in BMSCs promotes the formation of adipocytes, leading to avascular necrosis of the femoral head [11]. Hormones promote adipogenesis by activating C/EBPα, a crucial transcriptional regulator of fat production, through binding with glucocorticoid receptors.

Our previous research on the continuous regulation of BMSC adipogenic differentiation through C/EBPα control of PPARγ revealed that C/EBPα can participate in the adipogenic differentiation of BMSCs and inhibit osteogenic differentiation by upregulating PPARγ [12]. ChIP experiments have demonstrated that histone H3K27 acetylation in the PPARγ promoter region plays a crucial role in the epigenetic mechanism of SANFH. By inhibiting histone deacetylases (HDACs), C/EBPα increases the level of histone H3K27 acetylation in the PPARγ promoter region, thereby promoting the sustained expression of PPARγ. These findings suggest that histone

acetylation of PPARγ plays a significant role in glucocorticoid-induced BMSC adipogenic differentiation.

Histone acetylation is regulated by two enzyme families, histone acetyltransferases (HATs) and HDACs, with opposite effects [13]. HDACs have been shown to be involved in osteogenesis and adipogenesis [14]. Some HDACs can modulate chromatin structure and alter the transcriptional activity of osteoblast-related genes [15]. Studies indicate that DNA methylation and histone acetylation are associated with PPARγ in the regulation of MSC differentiation, suggesting that the status of DNA methylation and histone acetylation has potential for adipogenesis [16, 17]. Histone acetylation directly regulates the expression of PPARγ, as a significant increase in histone H3K9 acetylation levels in the PPARγ enhancer region leads to increased PPARγ expression [18, 19].

Our research team previously demonstrated that C/EBPα inhibits the expression of HDACs, leading to histone acetylation modification of PPARγ, but specific HDAC validation is lacking. Currently, research on the corresponding mechanisms and pathways of HDACs in SANFH is limited, with a focus mostly on cellular validation and a lack of integration with animal and clinical studies. This study aims to combine cell, animal, and clinical specimen experiments with molecular biology techniques to screen for specific differentially expressed HDAC genes in BMSC adipogenic differentiation cell models. Moreover, we collected femoral heads from patients with SANFH and femoral neck fractures and validated the corresponding differentially expressed HDAC genes through H&E staining and immunohistochemistry. The aim of this research was to provide scientific evidence and key molecular targets for establishing molecular-level prevention and treatment strategies for SANFH.

Materials and methods

Clinical sample collection

In this study, SANFH patients composed the experimental group, and patients with femoral neck fractures composed the control group. A total of 16 femoral head samples were collected, including samples from 6 patients with SANFH (3 males and 3 females) and 10 patients with femoral neck fractures (5 males and 5 females). All enrolled patients were selected from those who underwent hip arthroplasty at the Department of Joint and Sports Medicine of Wuhan University Zhongnan Hospital between September 2021 and September 2022. Patients and their families were fully informed before the operation of all femoral head samples, with the consent of patients and their families, and the informed consent of biological specimens was signed. The study protocol was approved by the Medical Ethics Committee of Zhongnan Hospital of Wuhan University (Approval No: 2024044 K), and all experiments were performed in accordance with relevant guidelines and regulations.

Animals

Wuhan Wanqian Jiaxing Biotechnology Co., Ltd. (Wuhan, China) provided sixteen adult female C57BL/6 mice (6–8 weeks old, weighing 25–30 g). Animal care experts at the Wuhan University Animal Experimental Center maintained all the animals under normal conditions with regular feeding. The facility is equipped with an air filtration system, allowing the animals to move freely within their cages. All the animal experimental procedures were approved by the Experimental Animal Welfare Ethics Committee of Zhongnan Hospital of Wuhan University (Approval No. ZN2023062), and all the experiments were performed in accordance with relevant guidelines and regulations.

Model building of SANFH

Female C57BL/6 mice aged 8 weeks ($n=5$ per group) were intraperitoneally injected with lipopolysaccharide (LPS; Sigma–Aldrich, America; 20 mg/kg/d) for 2 days, followed by intramuscular injections of methylprednisolone (MPS; Pfizer, China; 40 mg/kg) five times per week for 4 weeks to induce glucocorticoid-associated osteonecrosis of the femoral head (GA-ONFH). The control group received an equal volume of saline solution.

Cell culture

Rat bone marrow mesenchymal stem cells (R-BMSCs) (Procell, Wuhan) were cultured in α-MEM (α-minimum essential medium) supplemented with 10% FBS (BI foetal bovine serum, US origin, 04-001-1ACS), 1% penicillin–streptomycin solution, and 100× (Biosharp, BL505A) and then cultured at 37 °C in a 5% CO2 cell culture incubator.

Cell grouping

The 3rd to 5th passages of R-BMSC cells (P3 − P5) were used for the cell experiments. When the cell density reached over 80% confluence during culture, the cells were grouped on the basis of whether dexamethasone (DEX) was added to the culture medium and the duration of DEX-induced BMSC adipogenic differentiation (OriCell, RAXMX-90031). The cells were divided into the following groups: control group, supplemented with complete culture medium; 4-day or 8-day hormone groups, containing complete culture medium supplemented with 10–6 mmol/L dexamethasone for 4 days or 8 days. Analyses of the control group and 4-day group are described in Sect. 2.10.

Oil red O staining

At 0, 4, and 8 days of dexamethasone-induced differentiation of the R-BMSCs, the cells from each group were

removed, the dexamethasone adipogenic induction culture medium was removed, and the 4% PFA fixative (Biosharp, BL539A) was applied for 20–30 min. After removing the fixative, 60% isopropanol was added for 5 min. The ORO staining working solution was prepared by mixing Oil Red O storage solution (OriCell, OILR-10001) with distilled water at a 3:2 ratio. After mixing, the mixture was centrifuged at 250×g for 4 min, and the supernatant was collected. After removing the isopropanol, freshly prepared working solution was added, and the mixture was incubated for 20 min. After 1 min of treatment with ORO buffer, the solution was discarded. The stained images of each group were observed under an optical microscope and recorded.

Protein extraction and Western blot analysis

At 0, 4, and 8 days of dexamethasone-induced BMSC adipogenic differentiation, proteins were extracted from the cells in each group. The cells were then placed in RIPA buffer (Beyotime, P0013B) supplemented with phenylmethylsulphonyl fluoride (PMSF, Beyotime, ST506) and lysed on ice for 30 min. The protein sample concentration (Absin, abs9232) was determined using the BCA method. Finally, an appropriate amount of SDS–PAGE protein loading buffer (Biosharp, BL511B) was added, and the mixture was boiled for 5–10 min. The detailed steps for protein blotting and extraction have been described elsewhere [20]. The primary antibodies used included rabbit anti-β-actin (Proteintech, 20536-1-AP, 1:1000), rabbit anti-PPARγ (Proteintech, 16643-1-AP, 1:1000), rabbit anti-C/EBPα (Abcam, ab40764, 1:1000), rabbit anti-FABP4 (Proteintech, 12802-1-AP, 1:1000), rabbit anti-COL1A1 (Proteintech, 67288-1-Ig, 1:1000), rabbit anti-RUNX2 (Proteintech, 20700-1-AP, 1:1000), and rabbit anti-OCN (Abcam, ab93876, 1:1000) antibodies. β-actin was used as a loading control. Visualization of the protein bands was accomplished with an enhanced chemiluminescence (ECL) reagent (Biosharp, BL523A). ImageJ software was used for quantitative analysis of the target protein bands, which were normalized to the loading control.

Real-time fluorescent quantitative PCR (RT–qPCR)

Total RNA was extracted using the PureLinkTM RNA Mini Kit (Invitrogen, 12183018 A). Genomic DNA was extracted using a specific DNase (Thermo Scientific, K2981), and cDNA was obtained using the Revert Aid RT Kit (Thermo Scientific, K1691). The mRNA was subsequently quantified in real-time using a Bio-Rad CFX96Touch real-time fluorescent quantitative PCR instrument and SYBR Colour qPCR combination (Vazyme, Jiangsu, China). The primers are listed in Supplementary Data 1 Table 1. The relative mRNA levels were determined using the comparative $2-\Delta\Delta Ct$ method. After PCR, Bio-Rad CFX Maestro software was used to calculate the relative expression levels of various genes using the $2-\Delta\Delta Ct$ method, with β-actin serving as the internal reference standard.

Chromatin immunoprecipitation assay (ChIP)

The detailed methods have been previously described [21]. We performed crosslinking and cell lysis, DNA sonication, immunoprecipitation, elution of protein-DNA complexes, de-crosslinking, and column-purifying DNA to obtain purified DNA, followed by the same experimental procedures described in 2.6. The primers are listed in Supplementary Data 1 Table 2.

Collection and Processing of clinical specimens

All clinical specimens were obtained from the femoral heads removed during hip arthroplasty at the Department of Joint and Sports Medicine of Wuhan University Zhongnan Hospital. After removal, the bone surfaces were rinsed with saline. A multifunctional cutting machine was used to cut the femoral head along the mid-coronal plane, with continuous saline irrigation during cutting to minimize heat generation affecting the bone.

Immunohistochemistry and H&E staining

The tissue samples were processed according to the methods described in reference [22]. Observations and analyses were performed via a Leica Aperio VERSA 8 system for microscopic scanning photographs and image acquisition.

RNA extraction, library preparation, sequencing, and data analysis

The RNA-seq experiments, high-throughput sequencing, and data analysis were conducted by SeqHealth Technology Co., Ltd. (Wuhan, China). Total RNA was extracted as described in Sect. 2.3 using TRIzol Reagent (Invitrogen, cat. NO 15596026) following previously described methods [23].

Statistical analysis

Data obtained from the experiments were statistically analysed using SPSS 26.0 software. The data are presented as the means ± standard deviations (x ± s). GraphPad Prism 9 software was used for statistical plotting. A P value < 0.05 was considered statistically significant.

Results

Bioinformatics analysis of RNA-seq data from DEX-stimulated BMSCs and the control group

Biological information analysis was performed using the RNA-seq data from DEX-stimulated BMSCs and the control group, resulting in the identification of 2133

upregulated and 1552 downregulated genes. Figure 1A shows the intragroup repeatability and intergroup differences of the sequencing samples, Fig. 1B shows a volcano plot, and Fig. 1C displays a heatmap of the DEGs. The GO enrichment analysis of the upregulated and downregulated DEGs revealed that DEX stimulation respectively promoted adipocyte differentiation (Fig. 1D) and inhibited osteoblast differentiation (Fig. 1E). A heatmap was generated for genes enriched in fat cell differentiation among the upregulated DEGs and genes enriched in osteoblast differentiation among the downregulated DEGs (Fig. 1F).

Gene expression changes during dexamethasone-induced adipogenic differentiation of BMSCs

P5 rat BMSCs were induced to undergo adipogenic differentiation with dexamethasone, simulating the hormonal effects on human BMSCs in vivo. The cells cultured for different durations were divided into 0-, 4-, and 8-day groups for subsequent experiments. The results from Oil Red O staining revealed that the cells in the 0-day group presented very few lipid droplets, whereas those in the 4-day group presented relatively small and lightly stained lipid droplets, and those in the 8-day group presented numerous lipid droplets, some of which were moderately fused and had larger volumes (Fig. 2A).

RNA from the three groups of cells was extracted for RT−qPCR experiments to validate the effect of

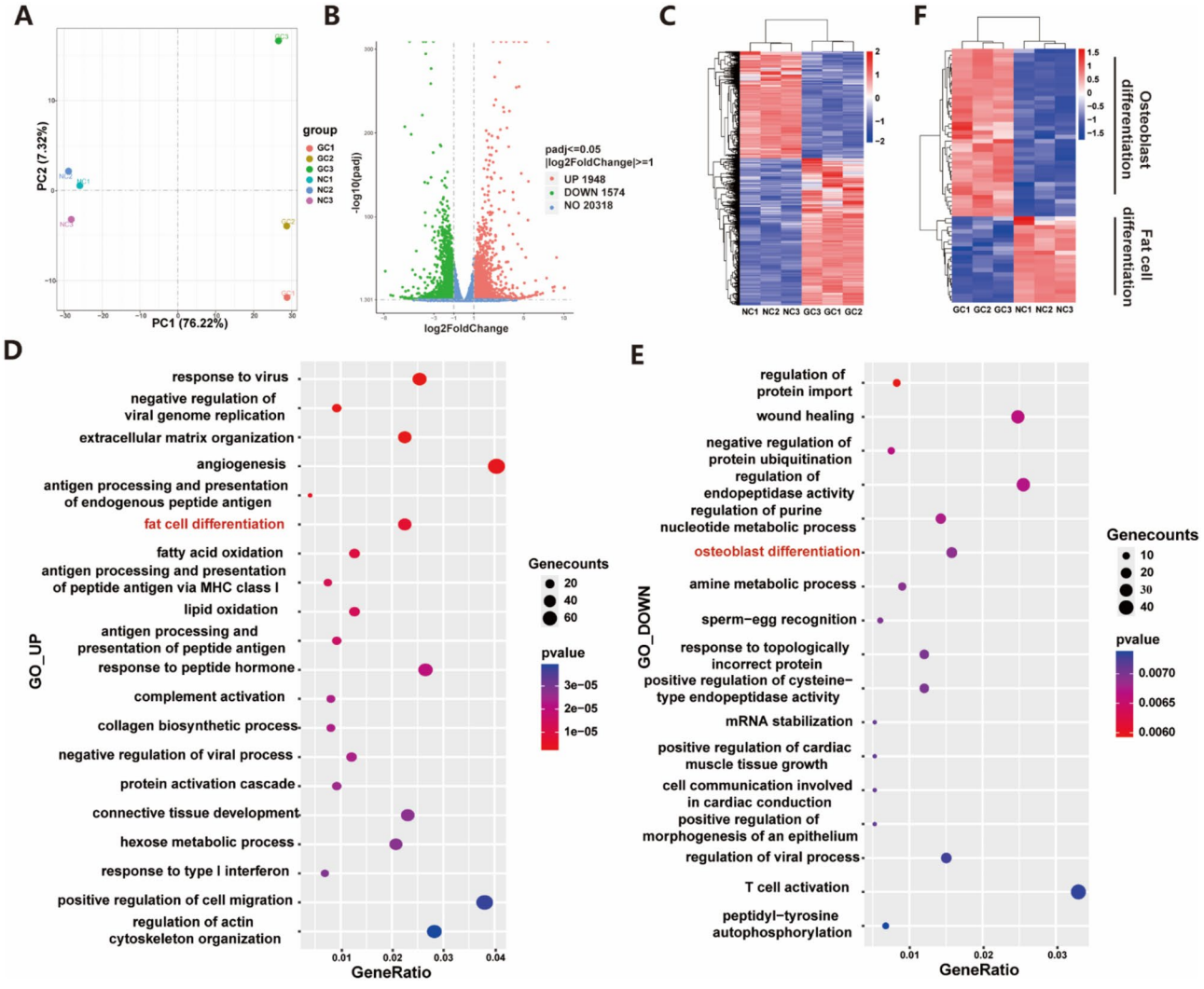

Fig. 1 Bioinformatics analysis of RNA-seq data from DEX-stimulated BMSCs and control BMSCs. **A**. PCA sample distribution of 4 control group samples and 4 hormone group samples. **B**. Volcano plot using the criteria |logFC| > 1 and adjusted p value < 0.05 (red dots represent upregulated genes, green dots represent downregulated genes). **C**. Heatmap showing the clustering relationship of DEGs between the control group and the DEX treatment group. **D**. GO enrichment analysis of upregulated DEGs. **E**. GO enrichment analysis of downregulated DEGs. **F**. Heatmap of genes enriched in fat cell differentiation among the upregulated DEGs and genes enriched in osteoblast differentiation among the downregulated DEGs

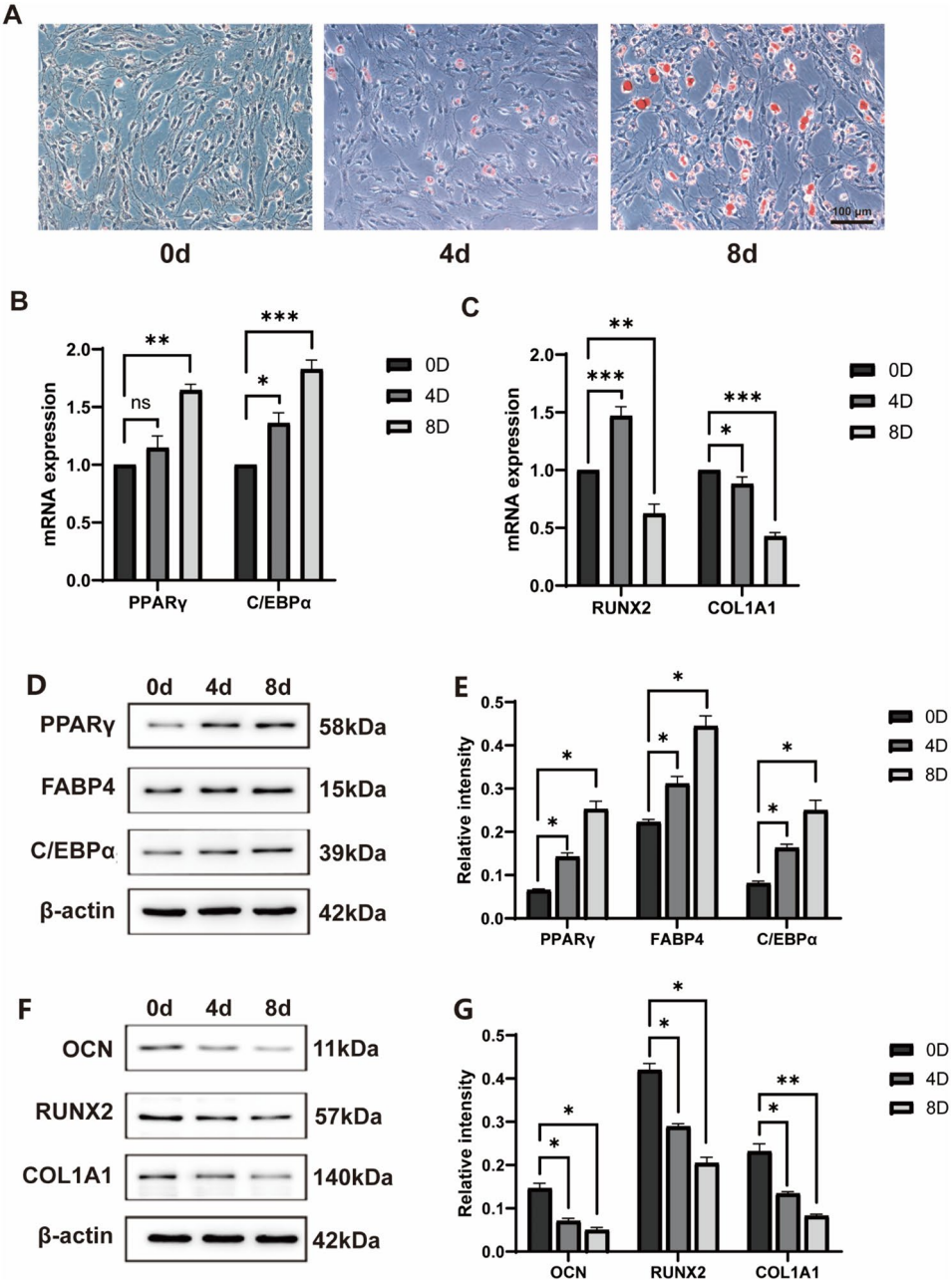

Fig. 2 Changes in gene expression during dexamethasone-induced adipogenic differentiation of BMSCs. **A**. Different time points of dexamethasone-induced adipogenic differentiation of BMSCs: 0 days, 4 days, and 8 days (100x). Scale bar: 100 μm. **B**: qPCR detection of adipogenic gene mRNA expression in BMSCs. **C**: qPCR detection of osteogenic gene mRNA expression in BMSCs. **D**, **E**: Protein expression of adipogenic genes in BMSCs; **F**, **G**: protein expression of osteogenic genes in BMSCs. (ns $p > 0.05$, * $p < 0.05$, ** $p < 0.01$, *** $p < 0.001$, compared with the 0-day group)

dexamethasone on the expression of adipogenic and osteogenic genes in rat BMSCs (Fig. 2B, C). The relative mRNA expression levels of adipogenic genes (PPARγ and C/EBPα) gradually increased in the 0-, 4-, and 8-day groups ($P<0.05$), whereas the relative mRNA expression levels of osteogenic genes (RUNX2 and COL1A1) gradually decreased ($P<0.05$).

Western blot analysis revealed that the expression levels of the adipogenic proteins PPARγ, C/EBPα, and FABP4 gradually increased ($P<0.05$) in the 0-, 4-, and 8-day groups, whereas the expression levels of the osteogenic proteins RUNX2, COL1A1, and OCN gradually decreased ($P<0.05$) (Fig. 2D, E, F, G).

Changes in HDAC expression in the adipogenic differentiation model of BMSCs

After the successful establishment of an in vitro adipogenic differentiation model of BMSCs, RNA from the

three groups of cells was extracted for RT−qPCR analysis (Fig. 3A). The results revealed a significant increase in the relative expression levels of HDAC 2, HDAC 3, and HDAC 8 mRNAs ($P<0.05$), whereas the relative expression levels of HDAC6 and HDAC10 decreased, with HDAC10 showing a significant decrease ($P<0.05$).

On the basis of the above experimental results, we selected HDAC10 as the target gene for this study.

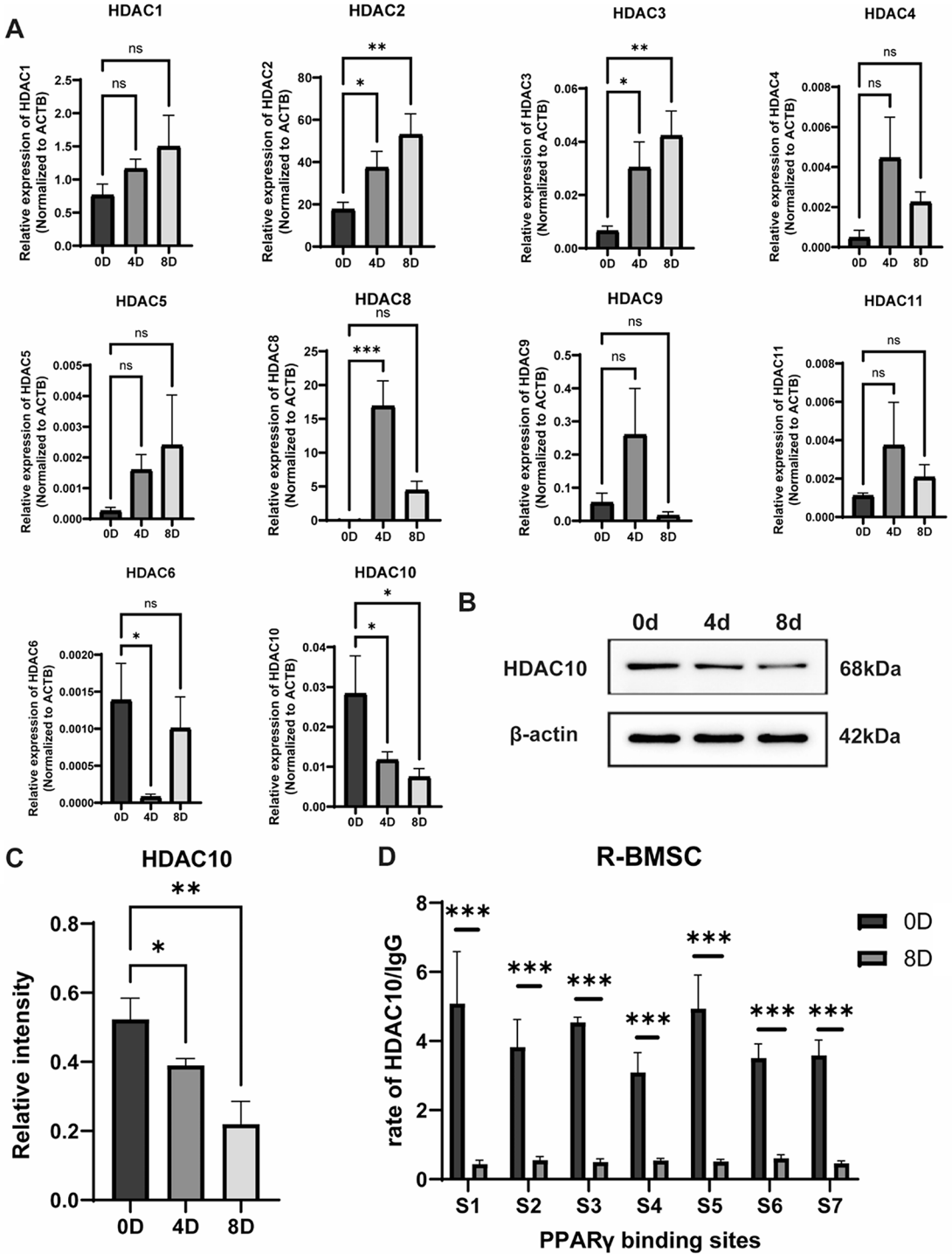

Fig. 3 Changes in HDAC expression in the adipogenic differentiation model of BMSCs. **A**. Changes in the expression of HDACs during dexamethasone-induced adipogenic differentiation of BMSCs. **B**, **C**: Changes in the protein expression of HDAC10 during dexamethasone-induced adipogenic differentiation of BMSCs. **D**. ChIP–qPCR results showing the reduced enrichment of HDAC10 at sites S1-S7. (ns $p>0.05$, * $p<0.05$, ** $p<0.01$, *** $p<0.001$, compared with the 0-day group)

Western blot analysis revealed that under dexamethasone induction, the expression level of HDAC10 gradually decreased ($P<0.05$) (Fig. 3B, C).

Next, we investigated the potential mechanism by which the transcription factor HDAC10 regulated PPARγ expression. Seven potential binding sites of HDAC10 were predicted within 2 kb upstream of the PPARγ transcription start site. ChIP experiments in BMSCs revealed DNA fragments bound to the transcription factor HDAC10, and RT−qPCR experiments were used to detect whether the obtained DNA fragments contained the promoter region of the PPARγ gene. Compared with that in the 0-day group, enrichment of HDAC10 in the potential binding sites S1-S7 of the PPARγ promoter region was significantly reduced at 8 days (Fig. 3D).

Imaging findings and general view of clinical specimens

In this study, imaging data and femoral head samples were collected from patients with steroid-associated necrosis of the femoral head (SANFH) and femoral neck fractures.

In terms of imaging, X-rays of SANFH patients (Fig. 4A) revealed significant local patchy sclerosis and cystic changes, whereas CT scans (Fig. 4B) revealed collapse and flattening of the femoral head. MRI images (Fig. 4D, E) revealed the double-line sign and localized signal intensity elevation within the femoral head. For femoral neck fractures, X-rays and CT scans (Fig. 4F, G) revealed obvious cortical fractures and displacement of the fracture ends.

The femoral heads of the SANFH group exhibited slight flattening, uneven surfaces, and black folds near the junction of the head and neck (Fig. 4C). The femoral heads of the femoral neck fractures appeared spherical with a

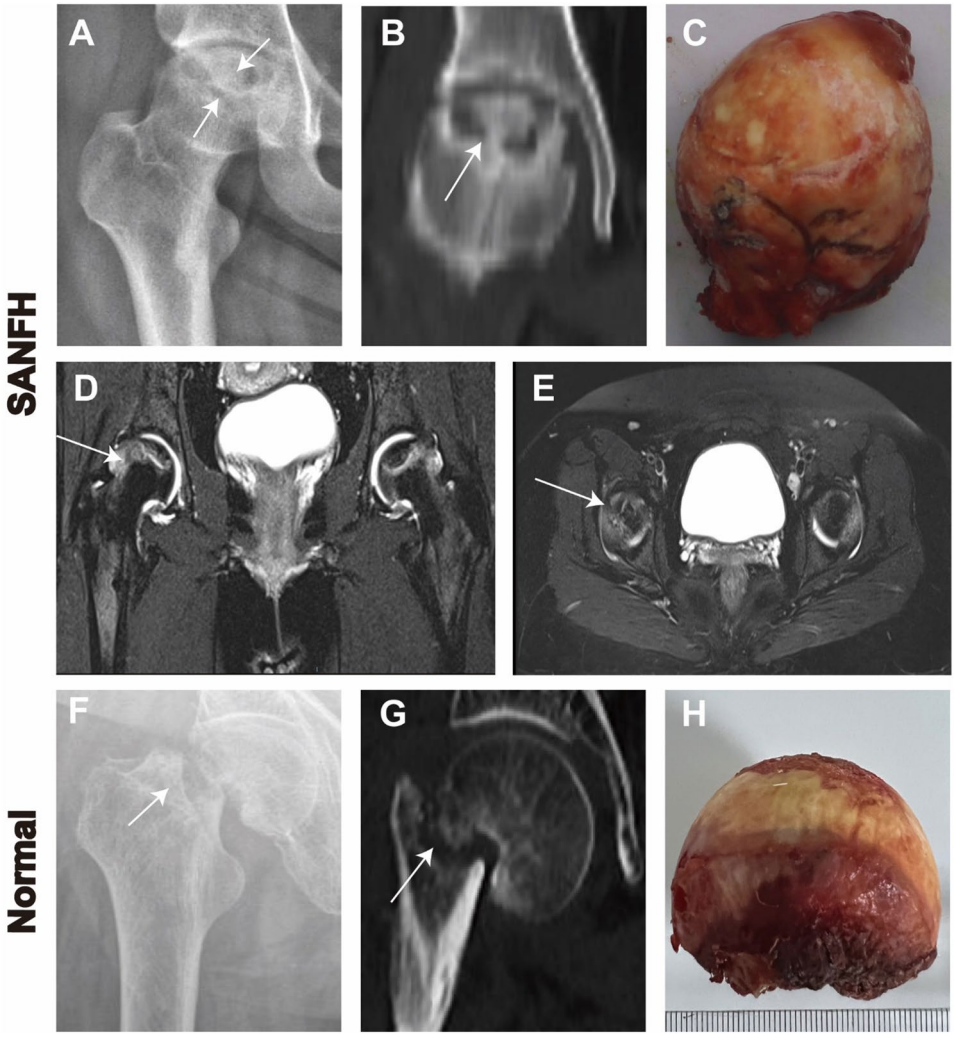

Fig. 4 Radiographic and gross appearances of the clinical samples. **A**, **B**, **C** represent the radiographic and specimen appearances of SANFH patients. **D**, **E** show the MRI findings of SANFH patients. **F**, **G**, **H** depict the radiographic and specimen appearances of femoral neck fractures

smooth surface, and blood infiltration was observed in the fracture area (Fig. 4H).

Histopathological findings in the animal specimens

To validate the differences in adipogenic and osteogenic gene expression in steroid-associated necrosis of the femoral head (SANFH) compared with normal femoral head specimens, we collected femoral heads from two groups of mice for IHC staining.

In the immunohistochemical sections, both groups presented varying degrees of positive expression of PPARγ, COL1A1, and OCN (Fig. 5A, E, C). Osteogenesis-related genes such as COL1A1 and OCN were expressed in the osteocytes between trabeculae in both groups, with significantly lower expression in the experimental group than in the control group (Fig. 5A, C). The adipogenesis-related gene PPARγ was expressed mainly in adipocyte-containing lipid droplets between trabeculae in the necrotic area of the experimental group and appeared brownish yellow (Fig. 5E). Statistical analysis revealed that the protein expression of PPARγ was significantly greater in the experimental group than in the control group ($P<0.05$) (Fig. 5F), whereas the protein expression of COL1A1 and OCN was lower in the experimental group than in the control group ($P<0.05$) (Fig. 5B, D).

We subsequently performed immunohistochemistry on mouse femoral head samples to analyse the expression of HDAC10 (Fig. 5G). HDAC10 was expressed in osteocytes and interstitial cells in both the control and experimental groups, with statistical analysis revealing a decrease in HDAC10 expression in the experimental group compared with the control group ($P<0.05$) (Fig. 5H). The experimental results were consistent with the results of the in vitro cell experiments.

Histopathological findings of the clinical specimens

To further verify the differences in adipogenic and osteogenic gene expression between SANFH specimens compared with normal femoral head specimens, we collected femoral heads from the two groups of patients for H&E and IHC staining.

H&E staining revealed that in the control group, the trabecular bone structure was intact, with abundant osteoblasts and few empty lacunae, and the adipocytes in the interstitium had a normal morphology. In the experimental group, the necrotic area presented abundant lacunar cells, destruction of adipocytes in the interstitium, and a large amount of uniformly stained necrotic tissue (Fig. 6A).

In the immunohistochemistry sections, positive expression of PPARγ, C/EBPα, COL1A1, OCN, and RUNX2 was observed to varying degrees in both groups (Fig. 6B, D, F, H, J). Osteogenic genes such as COL1A1, OCN, and RUNX2 were expressed in the trabecular bone and osteoblasts to a greater extent in the experimental than in the control group (Fig. 6B, D, F). Adipogenic genes such as PPARγ and C/EBPα were highly expressed

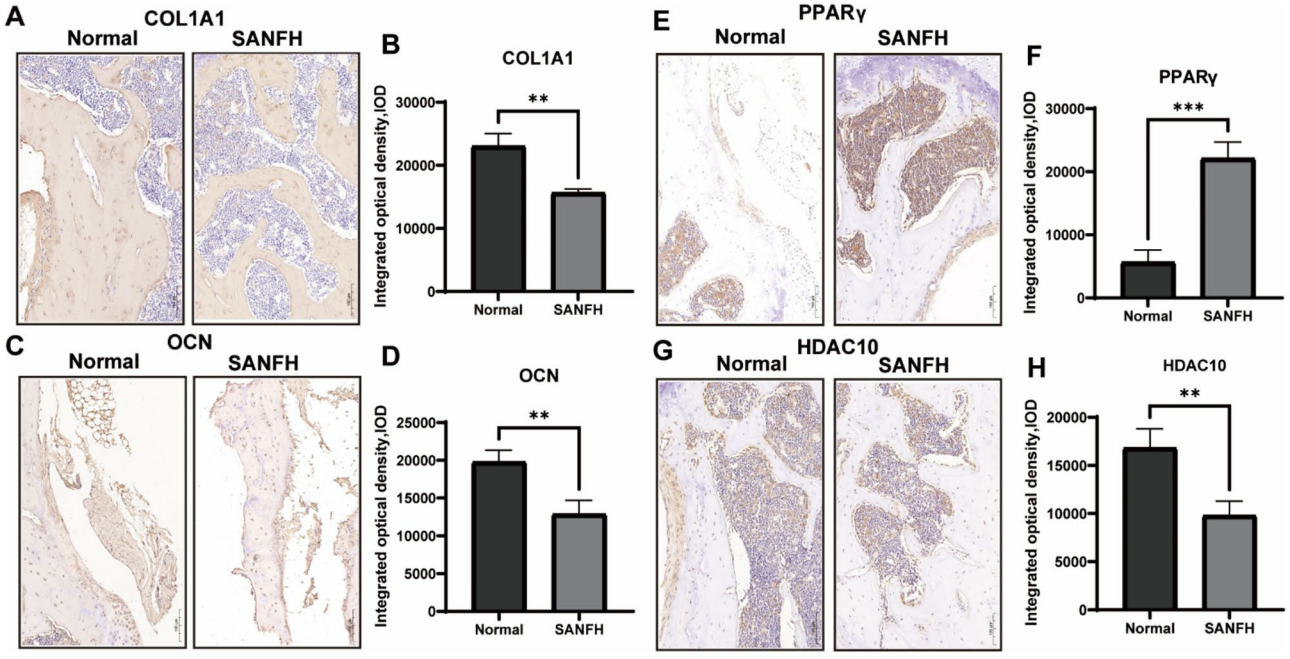

Fig. 5 **A**, **B**, **C**, **D**: IOD analysis comparing the expression of the osteogenic genes COL1A1 and OCN in specimens from both groups. **E**, **F**: IOD analysis comparing the expression of the adipogenic gene PPARγ in specimens from both groups. **G**, **H**: Differential expression of HDAC10 via immunohistochemistry between the control and experimental groups. (*$p<0.05$, **$p<0.01$, ***$p<0.001$ compared with the control group.) (30x)

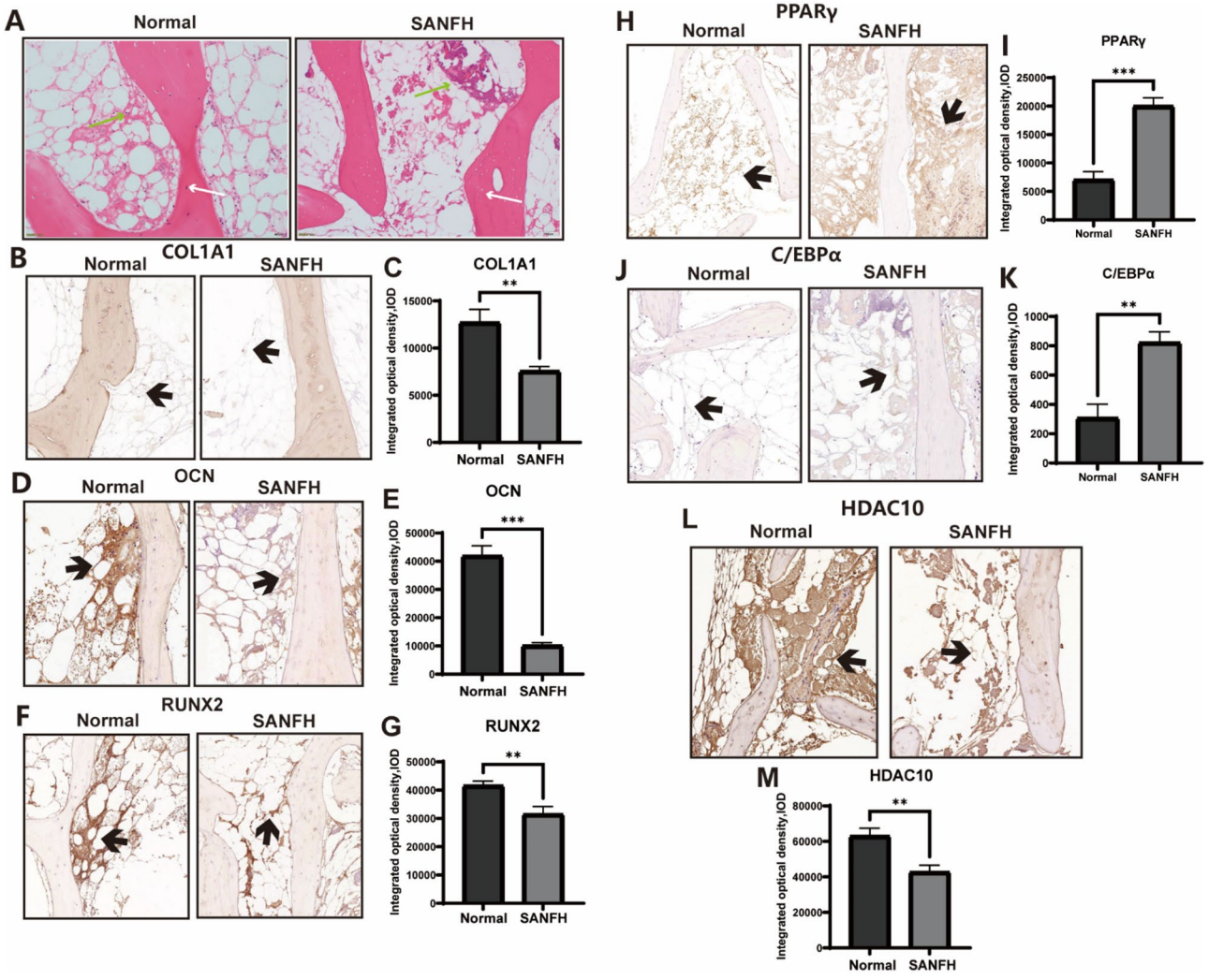

Fig. 6 **A**: Normal osteoblast morphology and intact interstitial adipocytes in the control group. Abundant lacunar cells and destruction of interstitial adipose tissue were observed in the experimental group. **B**, **C**, **D**, **E**, **F**, **G**: Analysis of the IOD of the osteogenic genes COL1A1, OCN, and RUNX2 in the two groups of specimens. **H**, **I**, **J**, **K**: Analysis of the IOD of the adipogenic genes PPARγ and C/EBPα in the two groups of specimens. **L**, **M**: Differential expression of HDAC10 according to immunohistochemistry in the control group and the experimental group. (*$p<0.05$, **$p<0.01$, compared with the control group) (100x)

mainly in adipocyte vacuoles in the necrotic area of the trabecular bone in the experimental group and appeared brownish yellow (Fig. 6H, J). Statistical analysis revealed that the protein expression of PPARγ and C/EBPα was significantly greater in the experimental group than in the control group ($P<0.05$), whereas the protein expression of COL1A1, OCN, and RUNX2 was lower in the experimental group than in the control group ($P<0.05$) (Fig. 6C, E, G, I, K).

We subsequently conducted immunohistochemistry on human femoral head samples to analyse the expression of HDAC10 (Fig. 6L). Compared with that in the control group, the expression of HDAC10 in the trabecular bone and interstitial cells was significantly lower in the experimental group compared with the control group ($P<0.05$) (Fig. 6M). The experimental results were consistent with those of the cell and animal experiments.

Discussion

The exact pathological process of steroid-induced avascular necrosis of the femoral head (SANFH) is not yet clear, but the theory of lipid metabolism disorder is currently recognized as the most likely core pathogenic mechanism [21]. Bone marrow mesenchymal stem cells (BMSCs) are present mainly in the bone marrow of cancellous bone, and under different induction conditions in vitro, BMSCs can differentiate into osteoblasts and adipocytes, among others [24]. Abnormal differentiation of BMSCs into adipocytes or osteoblasts is important in the pathogenesis of intraosseous fat accumulation [25].

Studies have shown that hormones significantly inhibit the osteogenic differentiation of BMSCs while promoting their adipogenic differentiation. A marked increase in intraosseous fat content leads to irreversible necrosis of the femoral head [26–28]. Under the influence of hormones, BMSCs inhibit osteogenic differentiation by suppressing the Wnt/β-catenin pathway while activating Wnt/β inhibitors such as DKK1 (dickkopf-1) and SFRPs. Additionally, hormone induction increases the expression of C/EBPβ and C/EBPδ, which bind to the promoter region of PPARγ and induce its expression. PPARγ activates many adipogenic-related genes, such as fatty acid binding protein 4 (FABP4), and the expression of C/EBPα. Subsequently, C/EBPα further promotes the expression of PPARγ, forming a positive feedback loop that promotes the adipogenic differentiation of BMSCs [29, 30].

In our preliminary research [20], we extracted primary rat BMSCs and induced adipogenesis to verify that adipogenic gene expression increased while osteogenic gene expression decreased under adipogenic conditions. Further experiments involving the overexpression and knockout of the C/EBPα and PPARγ genes confirmed that C/EBPα promoted BMSC adipogenic differentiation by targeting the PPARγ signalling pathway. Additionally, overexpression of C/EBPα impaired BMSC osteogenic differentiation. ChIP and dual-luciferase assays subsequently confirmed that C/EBPα directly regulated the activity of the PPARγ promoter, thus coregulating the process of adipogenesis.

In subsequent in vivo and in vitro experiments, we observed significant enrichment of H3K27ac at the PPARγ promoter region during adipogenic induction of BMSCs. Compared with the empty vector group, overexpression of C/EBPα also resulted in significant enrichment of H3K27ac, indicating that C/EBPα promoted acetylation of histone H3K27 at the PPARγ promoter region, mediating activation and sustained expression of the PPARγ gene and thus BMSCs towards adipogenic differentiation.

Further inhibition experiments using the natural compound curcumin, a histone acetyltransferase inhibitor, revealed a marked reduction in both PPARγ expression and adipogenic differentiation in BMSCs. Subsequent use of the classic HDAC inhibitor valproic acid (VPA) significantly increased PPARγ levels in BMSCs. Additionally, knocking out C/EBPα led to increased expression of HDAC1, suggesting that C/EBPα might promote sustained PPARγ expression by inhibiting HDAC and enhancing PPARγ acetylation. Preliminary studies have only begun to verify possible changes in HDAC1 expression. Broad-spectrum screening or multidirectional validation has not yet been conducted to confirm that specific HDAC gene alterations lead to persistent changes in the acetylation of H3K27 at the PPARγ promoter region, thereby contributing to the ongoing progression of femoral head necrosis.

In the field of epigenetics, histone modifications, such as those involving histone deacetylases (HDACs), can influence gene transcription by enhancing the interaction between DNA and histones, thereby affecting chromatin structure and consequently affecting the characteristics of mesenchymal stem cells, such as potency and differentiation [31]. Histone acetylation is associated with gene activation, whereas deacetylation is associated with gene silencing. Currently, 18 enzymes with deacetylase activity are known to exist in mammals. These 18 HDACs are typically classified into two categories: classical (Classes I, II, and IV) and sirtuins (Class III). The activity of classical HDACs depends on zinc ions (Zn2+), whereas sirtuins utilize nicotinamide adenine dinucleotide (NAD+) to function, exhibiting completely different mechanisms of action [32]. HDACs provide a link between signalling pathways for cell differentiation and transcription factors, playing a role in the regulation of various transcription factors and signalling pathways [33].

Research has shown that the levels of histone acetylation, especially the acetylation of lysine 9 on histone H3 (H3K9ac) and lysine 14 on histone H3 (H3K14ac), as well as the methylation of gene promoter DNA, are crucial for regulating osteogenic differentiation [34]. Additionally, the HDAC inhibitor valproic acid (VPA) can increase the levels of H3K9ac and the expression of osteogenic-related genes, including RUNX2, osteocalcin (OCN), and osteopontin, while regulating RUNX2 activity [15]. Knocking out the HDAC3 gene in class I HDACs reduces osteoblast levels and increases fat deposition in the bone marrow, severely impairing mouse skeletal health [35]. HDAC8 can inhibit the expression of osteogenic-related genes, and inhibition of HDAC8 with VPA promotes the osteogenic differentiation of rat BMSCs [36]. In cartilage ossification, class II HDACs also play a role by integrating the extracellular signals required for osteogenic differentiation with transcriptional regulatory factors [32]. Mice with HDAC4 deficiency can survive but exhibit premature cartilage ossification, leading to many skeletal defects, including vertebral fusion, reduced long bone length, and premature cranial ossification [37]. Conversely, transgenic expression of HDAC4 from the COL2A1 promoter inhibits chondrocyte maturation by blocking RUNX2 activity [38]. In the regulation of adipogenic differentiation, the level of histone acetylation is positively correlated with adipogenic differentiation. Multiple studies have shown that HDACs inhibit adipogenic differentiation by downregulating the level of histone acetylation [40]. HDAC1 and HDAC3 inhibit the expression of PPARγ and adipogenic differentiation [41]. ChIP-seq results indicate an enrichment of H3K27ac

in the PPARγ promoter region after 48 h of adipogenic induction, suggesting that H3K27ac likely participates in the process of adipogenic differentiation [42]. This conclusion is consistent with previous studies in this project showing decreased expression of H3K27ac after knocking out C/EBPα.

HDAC10 consists of 20 exons, comprising two alternatively spliced transcripts, along with N-terminal catalytic domains and C-terminal leucine-rich domains [43]. In addition to its deacetylase activity in the nucleus, HDAC10 may also inhibit transcriptional functions. It plays significant roles in cell proliferation, apoptosis, invasion, migration, metastasis, and angiogenesis in tumour cells. With respect to lipid metabolism, studies have reported reduced expression of HDAC10 in obese individuals and other animals, including mice and monkeys [44]. The phthalate ester butyl benzyl phthalate (BBP) can decrease HDACs, including HDAC10, and further promote H3K9ac modification, thereby driving adipogenesis in BMSCs [45]. However, research on the involvement of HDAC10 in BMSC adipogenic differentiation is currently limited and insufficient. This study revealed that HDAC10 expression continues to decrease during BMSC adipogenic differentiation, thereby promoting the sustained expression of PPARγ.

Conclusion

Here, we demonstrate the significant epigenetic role of HDAC10 in steroid-induced avascular necrosis of the femoral head (SANFH) using cell, animal and human experiments. Within the classical HDAC family, HDAC10 is significantly correlated with sustained adipogenic differentiation of BMSCs and a marked decrease in enrichment at the PPARγ promoter region. These findings suggest that HDAC10 may be involved in the occurrence of SANFH by regulating the histone acetylation of PPARγ. Taken together, these results provide a meaningful direction for future research on the epigenetic mechanisms and therapeutic approaches for this disease.

Supplementary Information

The online version contains supplementary material available at https://doi.org/10.1186/s13018-024-05121-z.

Supplementary Material 1

Supplementary Material 2

Author contributions

Y.Y. designed the study and wrote the manuscript. P.D. conducted the experiments and collected the data. L. Z. and J. X. provided expertise in the software analyses and helped interpret the data. Y. Y., P. D. and L. Z. were involved in the data analyses, validation, and methodology. Z.P. directed and supervised the project to ensure its success.

Funding

This study was supported by the National Natural Science Foundation of China (No. 81972066) and the Discipline Capacity Building Fund of Zhongnan Hospital of Wuhan University (No. KYXM2023006).

Data availability

No datasets were generated or analysed during the current study.

Declarations

Ethics approval and consent to participate

The study protocol was approved by the Medical Ethics Committee of Zhongnan Hospital of Wuhan University (Approval No: 2024044 K). All the animal experimental procedures were approved by the Experimental Animal Welfare Ethics Committee of Zhongnan Hospital of Wuhan University (Approval No. ZN2023062).

Competing interests

The authors declare no competing interests.

Author details

[1]Department of Orthopedics Trauma and Microsurgery, Zhongnan Hospital of Wuhan University, Wuhan 430071, China

Received: 24 April 2024 / Accepted: 26 September 2024
Published online: 12 October 2024

References

1. Mont MA, Cherian JJ, Sierra RJ, et al. Nontraumatic osteonecrosis of the femoral head: where do we stand today? A ten-year Update[J]. J Bone Joint Surg Am. 2015;97(19):1604–27.
2. Lespasio MJ, Sodhi N, Mont MA. Osteonecrosis of the Hip: A Primer. *Perm J*. 2019;23:18-100.
3. Mont MA, Salem HS, Piuzzi NS, et al. Nontraumatic osteonecrosis of the femoral head: where do we stand today ? A 5-Year Update[J]. J Bone Joint Surg Am. 2020;102(12):1084–99.
4. Migliorini F, La Padula G, Oliva F, et al. Operative management of avascular necrosis of the femoral head in skeletally immature patients: a systematic review. Life (Basel). 2022;12(2):179.
5. Sadile F, Bernasconi A, Russo S, et al. Core decompression versus other joint preserving treatments for osteonecrosis of the femoral head: a meta-analysis. Br Med Bull. 2016;118(1):33–49.
6. Quaranta M, Miranda L, Oliva F, Aletto C, Maffulli N. Osteotomies for avascular necrosis of the femoral head. Br Med Bull. 2021;137(1):98–111.
7. Migliorini F, Maffulli N, Eschweiler J, et al. Core decompression isolated or combined with bone marrow-derived cell therapies for femoral head osteonecrosis. Expert Opin Biol Ther. 2021;21(3):423–30.
8. Migliorini F, Maffulli N, Baroncini A, et al. Prognostic factors in the management of osteonecrosis of the femoral head: a systematic review. Surgeon. 2023;21(2):85–98.
9. Wang Q, Yang Q, Chen G, et al. LncRNA expression profiling of BMSCs in osteonecrosis of the femoral head associated with increased adipogenic and decreased osteogenic differentiation[J]. Sci Rep. 2018;8(1):9127.
10. Li Y, Jin D, Xie W, et al. PPAR-gamma and wnt regulate the differentiation of MSCs into adipocytes and osteoblasts Respectively[J]. Curr Stem Cell Res Ther. 2018;13(3):185–92.
11. Li J, Li Y, Wang Y, et al. Preventive effects of siRNA targeting PPARgamma gene on steroid-induced osteonecrosis in rabbits[J]. Connect Tissue Res. 2014;55(5–6):322–30.
12. Duan P, Wang H, Yi X, et al. C/EBPalpha regulates the fate of bone marrow mesenchymal stem cells and steroid-induced avascular necrosis of the femoral head by targeting the PPARgamma signalling pathway[J]. Stem Cell Res Ther. 2022;13(1):342.
13. Jang S, Hwang J, Jeong HS. The role of histone acetylation in mesenchymal stem cell Differentiation[J]. Chonnam Med J. 2022;58(1):6–12.
14. Boquest AC, Noer A, Collas P. Epigenetic programming of mesenchymal stem cells from human adipose tissue[J]. Stem Cell Rev. 2006;2(4):319–29.

15. Zhang YX, Sun HL, Liang H, et al. Dynamic and distinct histone modifications of osteogenic genes during osteogenic differentiation[J]. J Biochem. 2015;158(6):445–57.
16. Yi SA, Nam KH, Kim S et al. Vulpinic acid controls stem cell fate toward Osteogenesis and Adipogenesis[J]. Genes (Basel), 2019;11(1):18.
17. Zhao QH, Wang SG, Liu SX, et al. PPARgamma forms a bridge between DNA methylation and histone acetylation at the C/EBPalpha gene promoter to regulate the balance between osteogenesis and adipogenesis of bone marrow stromal cells[J]. FEBS J. 2013;280(22):5801–14.
18. Steger DJ, Grant GR, Schupp M, et al. Propagation of adipogenic signals through an epigenomic transition state[J]. Genes Dev. 2010;24(10):1035–44.
19. Sugii S, Evans RM. Epigenetic codes of PPARgamma in metabolic disease[J]. FEBS Lett. 2011;585(13):2121–8.
20. Duan P, Wang H, Yi X, Pan Z, et al. C/EBPα regulates the fate of bone marrow mesenchymal stem cells and steroid-induced avascular necrosis of the femoral head by targeting the PPARγ signalling pathway. Stem Cell Res Ther. 2022;13(1):342.
21. Wang L, Tian H, Jiang L et al. Disrupting circadian control of autophagy induces podocyte injury and proteinuria. *Kidney Int*. 2024;105(5):1020-1034.
22. Cheng Y, Chen H, Duan P, et al. Early depletion of M1 macrophages retards the progression of glucocorticoid-associated osteonecrosis of the femoral head. Int Immunopharmacol. 2023;122:110639. 2023.110639.
23. Liu K, Xie B, Peng L, Wu Q, Hu J. Profiling of RNA editing events in plant organellar transcriptomes with high-throughput sequencing. *Plant J*. 2024;118(2):345-357.
24. Chang C, Greenspan A, Gershwin ME. The pathogenesis, diagnosis and clinical manifestations of steroid-induced osteonecrosis[J]. J Autoimmun. 2020;110:102460.
25. Derubeis AR, Cancedda R. Bone marrow stromal cells (BMSCs) in bone engineering: limitations and recent advances[J]. Ann Biomed Eng. 2004;32(1):160–5.
26. Han L, Wang B, Wang R, et al. The shift in the balance between osteoblastogenesis and adipogenesis of mesenchymal stem cells mediated by glucocorticoid receptor[J]. Stem Cell Res Ther. 2019;10(1):377.
27. Yu Z, Fan L, Li J, et al. Lithium prevents rat steroid-related osteonecrosis of the femoral head by beta-catenin activation[J]. Endocrine. 2016;52(2):380–90.
28. Cui Q, Jo WL, Koo KH, et al. ARCO Consensus on the pathogenesis of non-traumatic osteonecrosis of the femoral Head[J]. J Korean Med Sci. 2021;36(10):e65.
29. Park HW, Kim YC, Yu B, et al. Altern Wnt Signal Activates YAP/TAZ[J] Cell. 2015;162(4):780–94.
30. Ali AT, Hochfeld WE, Myburgh R, et al. Adipocyte and adipogenesis[J]. Eur J Cell Biol. 2013;92(6–7):229–36.
31. Strahl BD, Allis CD. The language of covalent histone modifications[J]. Nature. 2000;403(6765):41–5.
32. Lawlor L, Yang XB. Harnessing the HDAC-histone deacetylase enzymes, inhibitors and how these can be utilised in tissue engineering[J]. Int J Oral Sci. 2019;11(2):20.
33. Zhou Y, Peng J, Jiang S. Role of histone acetyltransferases and histone deacetylases in adipocyte differentiation and adipogenesis[J]. Eur J Cell Biol. 2014;93(4):170–7.
34. Wang J, Wang CD, Zhang N, et al. Mechanical stimulation orchestrates the osteogenic differentiation of human bone marrow stromal cells by regulating HDAC1[J]. Cell Death Dis. 2016;7(5):e2221.
35. Razidlo DF, Whitney TJ, Casper ME, et al. Histone deacetylase 3 depletion in osteo/chondroprogenitor cells decreases bone density and increases marrow fat[J]. PLoS ONE. 2010;5(7):e11492.
36. Fu Y, Zhang P, Ge J, et al. Histone deacetylase 8 suppresses osteogenic differentiation of bone marrow stromal cells by inhibiting histone H3K9 acetylation and RUNX2 activity[J]. Int J Biochem Cell Biol. 2014;54:68–77.
37. Nakatani T, Chen T, Johnson J, et al. The deletion of Hdac4 in mouse osteoblasts influences both Catabolic and Anabolic effects in Bone[J]. J Bone Min Res. 2018;33(7):1362–75.
38. Vega RB, Matsuda K, Oh J, et al. Histone deacetylase 4 controls chondrocyte hypertrophy during skeletogenesis[J]. Cell. 2004;119(4):555–66.
39. Lee JE, Schmidt H, Lai B et al. Transcriptional and epigenomic regulation of Adipogenesis[J]. *Mol Cell Biol*. 2019;39(11):e00601-18.
40. Lai B, Lee JE, Jang Y, et al. MLL3/MLL4 are required for CBP/p300 binding on enhancers and super-enhancer formation in brown adipogenesis[J]. Nucleic Acids Res. 2017;45(11):6388–403.
41. Kuzmochka C, Abdou HS, Hache RJ, et al. Inactivation of histone deacetylase 1 (HDAC1) but not HDAC2 is required for the glucocorticoid-dependent CCAAT/enhancer-binding protein alpha (C/EBPalpha) expression and preadipocyte differentiation[J]. Endocrinology. 2014;155(12):4762–73.
42. Brown JD, Feldman ZB, Doherty SP, et al. BET bromodomain proteins regulate enhancer function during adipogenesis[J]. Proc Natl Acad Sci U S A. 2018;115(9):2144–9.
43. Tong JJ, Liu J, Bertos NR, et al. Identification of HDAC10, a novel class II human histone deacetylase containing a leucine-rich domain[J]. Nucleic Acids Res. 2002;30(5):1114–23.
44. Qian H, Chen Y, Nian Z, et al. HDAC6-mediated acetylation of lipid droplet-binding protein CIDEC regulates fat-induced lipid storage[J]. J Clin Invest. 2017;127(4):1353–69.
45. Sonkar R, Powell CA, Choudhury M. Benzyl butyl phthalate induces epigenetic stress to enhance adipogenesis in mesenchymal stem cells[J]. Mol Cell Endocrinol. 2016;431:109–22.

Publisher's note